Chapter 2 Climate Change

2.1 Changes in temperature[12]

- The annual anomaly of the global average surface temperature in 2018 was the 4th highest since 1891. On a longer time scale, it is virtually certain that the annual global average surface temperature has risen at rates of 0.73ºC per century.
- The annual anomaly of the average temperature over Japan was the 6th highest since 1898. On a longer time scale, it is virtually certain that the annual average temperature over Japan has risen at rates of 1.21ºC per century.
- It is virtually certain that the annual number of days with maximum temperatures of 35 ºC or higher ($T_{max} \geq 35$ºC) and that with minimum temperatures of 25ºC or higher ($T_{min} \geq 25$ºC) have increased, while the annual number of days with minimum temperatures below 0ºC ($T_{min} < 0$ºC) has decreased.

2.1.1 Global surface temperature

The annual anomaly of the global average surface temperature in 2018 (i.e., the combined average of the near-surface air temperature over land and the SST) was +0.31ºC above the 1981 – 2010 average. This was the 4th highest since 1891. The global average temperature fluctuates on different time scales ranging from years to decades. On a longer time scale, it is virtually certain that the global average surface temperature has risen at a rate of 0.73ºC per century[13] (statistically significant at a confidence level of 99%[14]).

The surface temperature anomalies over the Northern Hemisphere and the Southern Hemisphere were +0.41ºC (the 4th highest) and +0.20ºC (the 4th highest) above the 1981 – 2010 average, respectively (Figure 2.1-1). It is virtually certain that average surface temperatures over the Northern Hemisphere and the Southern Hemisphere have risen at rates of 0.79 and 0.69ºC per century, respectively (both statistically significant at a confidence level of 99%).

Linear temperature trends for 5° × 5° latitude/longitude grid boxes indicate that most areas of the world, especially in the high latitudes of the Northern Hemisphere, have experienced long-term warming (Figure 2.1-2). These long-term trends in annual average temperatures can be largely attributed to global warming caused by increased concentrations of greenhouse gases such as CO_2. On a shorter time scale, temperatures fluctuate due to the influence of natural climate dynamics over different time scales ranging from years to decades.

12 Monthly, seasonal and annual estimates of average temperatures around the globe and around Japan are published on JMA's website.
https://www.data.jma.go.jp/cpdinfo/temp/index.html (Japanese)
https://ds.data.jma.go.jp/tcc/tcc/products/gwp/gwp.html (English)

13 According to IPCC AR5, the global average surface temperature has risen about 0.85°C (The 90% uncertainty interval is 0.65 to 1.06°C) over the period 1880 to 2012. The values given in IPCC AR5 and those in this report are considered to show no remarkable difference that have risen on a longer time scale and are higher since the mid-1990s, although they do not correspond exactly because of differences in dataset calculation methods and the statistical period examined.

14 For evaluation and clarification of the significance statistics used here, see "Explanatory note on detection of statistical significance in long-term trends" at the end of the report.

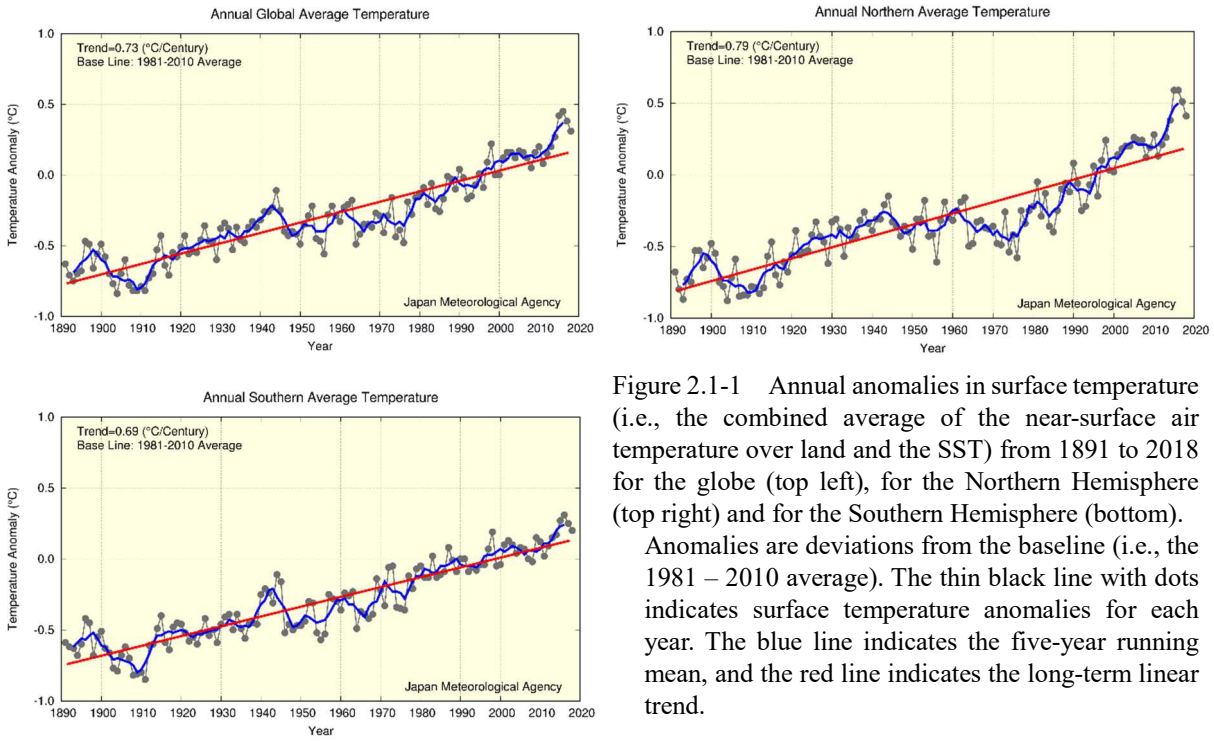

Figure 2.1-1 Annual anomalies in surface temperature (i.e., the combined average of the near-surface air temperature over land and the SST) from 1891 to 2018 for the globe (top left), for the Northern Hemisphere (top right) and for the Southern Hemisphere (bottom).
Anomalies are deviations from the baseline (i.e., the 1981 – 2010 average). The thin black line with dots indicates surface temperature anomalies for each year. The blue line indicates the five-year running mean, and the red line indicates the long-term linear trend.

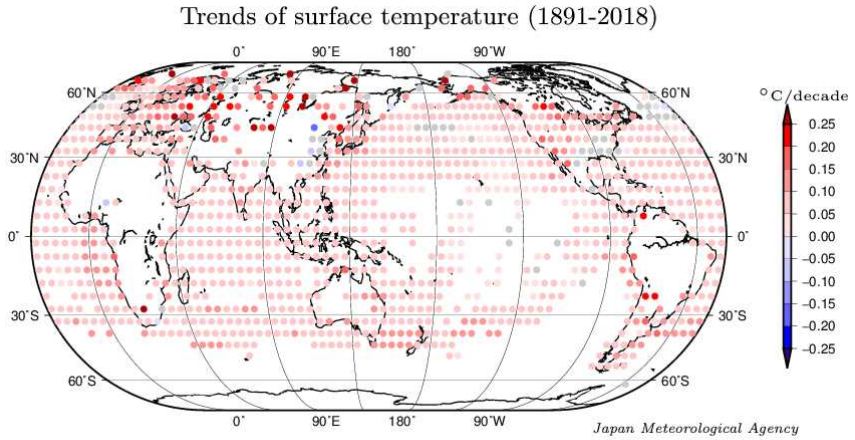

Figure 2.1-2 Linear temperature trends for 5° × 5° latitude/longitude grid boxes for the period of 1891 to 2018
The grid boxes with gray circles have no statistically significant trend (not statistically significant at a confidence level of 90%). Blank areas indicate those with insufficient data to analyze long-term trends.

2.1.2 Surface temperature over Japan

Long-term changes in the surface temperature over Japan are analyzed using observational records dating back to 1898. Table 2.1-1 lists the meteorological stations whose data are used to derive annual mean surface temperatures.

Table 2.1-1 Observation stations whose data are used to calculate surface temperature anomalies over Japan
Miyazaki and Iida were relocated in May 2000 and May 2002, respectively, and their temperatures have been adjusted to eliminate the influence of the relocation.

Element	Observation stations
Temperature (15 stations)	Abashiri, Nemuro, Suttsu, Yamagata, Ishinomaki, Fushiki, Iida, Choshi, Sakai, Hamada, Hikone, Tadotsu, Miyazaki, Naze, Ishigakijima

The mean surface temperature in Japan for 2018 is estimated to have been 0.68ºC above the 1981 – 2010 average, which is the 6th highest since 1898 (Figure 2.1-3). The surface temperature fluctuates on different time scales ranging from years to decades. On a longer time scale, it is virtually certain that the annual mean surface temperature over Japan has risen at a rate of 1.21ºC per century (statistically significant at a confidence level of 99%). Similarly, it is virtually certain that the seasonal mean temperatures for winter, spring, summer and autumn have risen at rates of about 1.10, 1.45, 1.11 and 1.20ºC per century, respectively (all statistically significant at a confidence level of 99%).

It is noticeable from Figure 2.1-3 that the annual mean temperature remained relatively low before the 1940s, started to rise and reached a local peak around 1960, entered a cooler era through to the mid-1980s and then began to show a rapid warming trend in the late 1980s. The warmest years on record have all been observed since the 1990s.

The high temperatures seen in recent years have been influenced by fluctuations over different time scales ranging from years to decades, as well as by global warming resulting from increased concentrations of greenhouse gases such as CO_2.

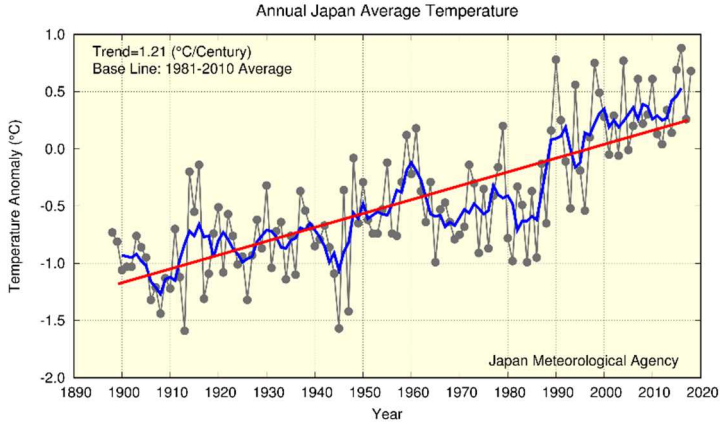

Figure 2.1-3 Annual surface temperature anomalies from 1898 to 2018 in Japan.
Anomalies are deviations from the baseline (i.e., the 1981 – 2010 average). The thin black line indicates the surface temperature anomaly for each year. The blue line indicates the five-year running mean, and the red line indicates the long-term linear trend.

2.1.3 Long-term trends of extreme temperature events[15] in Japan

This section describes long-term trends of extremely high/low-temperature events in Japan, as derived from analysis of temperature records from the 15 observation stations. Though monthly mean temperatures of the stations in Miyazaki and Iida have been adjusted to eliminate the influence of their relocation, records from these two stations are not used for analysis of daily temperatures due to the difficulty of adjustment in regard to the relocation.

(1) Long-term trends of monthly extreme temperatures

It is virtually certain that the frequency of extremely high monthly temperatures has increased, while that of extremely low monthly temperatures has decreased (both statistically significant at the confidence level of 99%) (Figure 2.1-4). The frequency of extremely high monthly temperatures has largely increased since about 1990.

15 Here, judgment of extremely high/low temperatures is based on the fourth-highest/lowest monthly values on records over the 118-year period from 1901 to 2018. The frequency of occurrence of the highest/lowest to the fourth-highest/lowest values over this period is once approximately every 30 years, which is close to JMA's definition of extreme climate events as those occurring once every 30 years or longer (See the Glossary for terms relating to Extreme climate event).

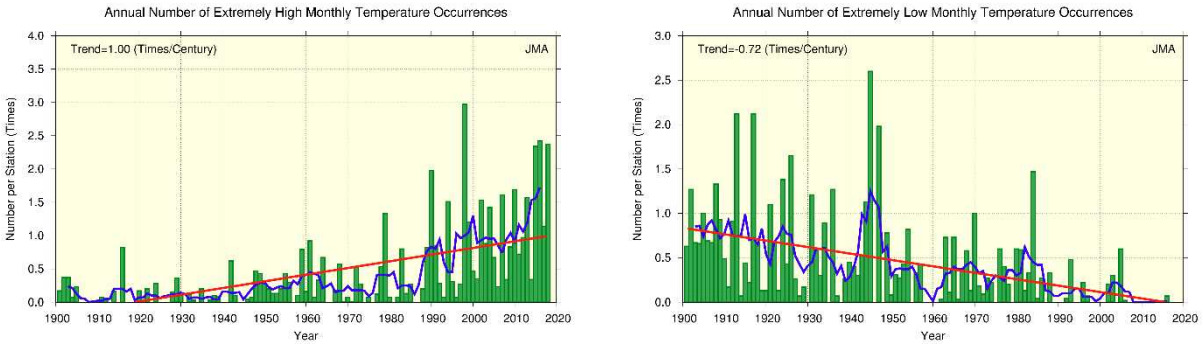

Figure 2.1-4 Annual number of extremely high/low monthly mean temperature occurrences from 1901 to 2018
The graphs show the annual number of occurrences of the highest/lowest first-to-forth values for each month during the period from 1901 to 2018. The green bars indicate annual occurrences of extremely high/low monthly mean temperatures divided by the total number of monthly observation data sets available for the year (i.e., the average occurrence per station). The blue line indicates the five-year running mean, and the straight red line indicates the long-term linear trend.

(2) Annual number of days with maximum temperatures of ≥ 30°C and ≥ 35°C

The annual number of days with maximum temperatures (T_{max}) of ≥ 30°C and T_{max} ≥ 35°C is virtually certain to have increased (both statistically significant at a confidence level of 99%) (Figure 2.1-5). Especially, the annual number of days with T_{max} ≥ 35°C has largely increased since about mid-1990s.

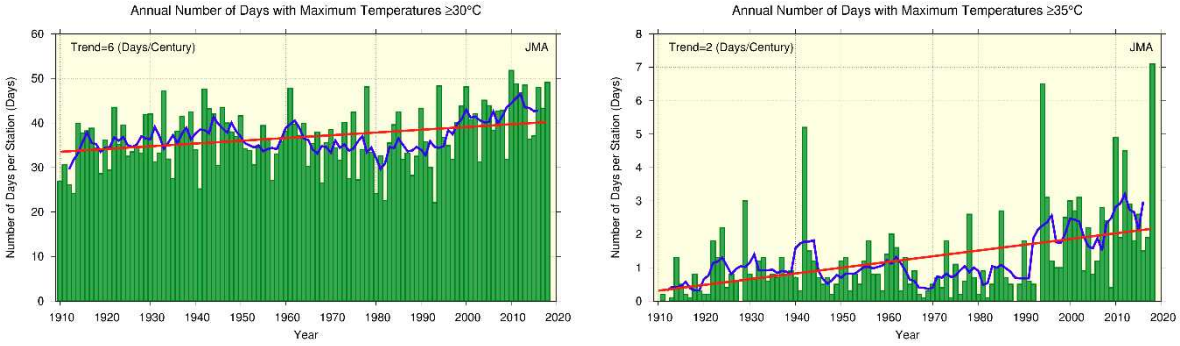

Figure 2.1-5 Annual number of days with maximum temperatures of ≥ 30°C and ≥ 35°C from 1910 to 2018
The green bars indicate the annual number of days per station for each year. The blue line indicates the five-year running mean, and the straight red line indicates the long-term linear trend.

(3) Annual number of days with minimum temperatures of < 0°C and ≥ 25°C

It is virtually certain that the annual number of days with minimum temperatures (T_{min}) of < 0°C has decreased, while the annual number of days with T_{min} ≥ 25°C has increased (both statistically significant at a confidence level of 99%) (Figure 2.1-6).

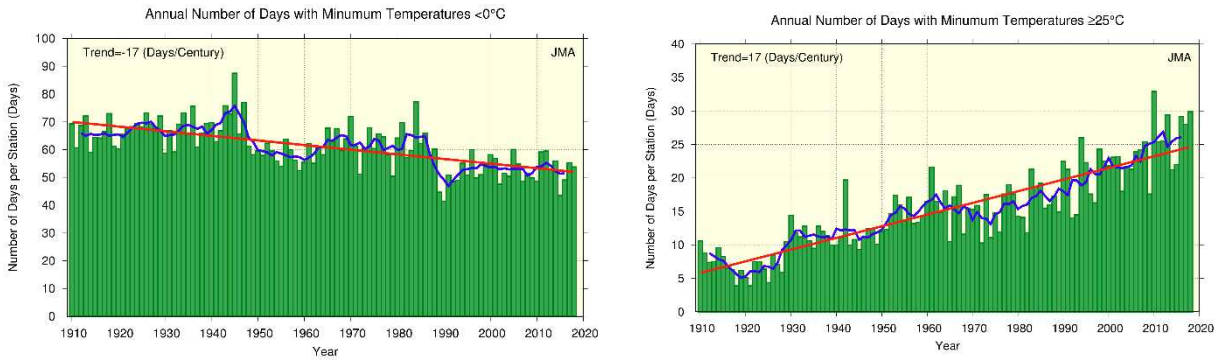

Figure 2.1-6 Annual number of days with minimum temperatures of ＜0°C and ≥ 25°C from 1910 to 2018
As per Figure 2.1-5.

2.1.4 Urban heat island effect at urban stations in Japan

The long-term trends of annual average temperatures are more pronounced for urban observation stations whose data are homogeneous over a long period (Sapporo, Sendai, Niigata, Tokyo, Yokohama, Nagoya, Kyoto, Osaka, Hiroshima, Fukuoka, Kagoshima) than for the average of the 15 rural observation stations (Table 2.1-2 and Figure 2.1-7).

Table 2.1-2 Long-term trends of annual and seasonal average temperatures at urban stations in Japan
These figures are based on data from 1927 to 2018. The trend of the 15 rural station averages (Table 2.1-1) is also listed. Values shown in italics are not statistically significant at a confidence level of 90%. For stations with asterisks (5 urban stations, and Iida and Miyazaki among the 15 rural stations), trends are calculated after adjustment to eliminate the influence of relocation.

Station	Long-term temperature trend (°C/century)														
	Average					Daily maximum					Daily minimum				
	Ann	Win	Spr	Sum	Aut	Ann	Win	Spr	Sum	Aut	Ann	Win	Spr	Sum	Aut
Sapporo	2.6	3.3	2.8	1.7	2.4	0.9	1.5	1.5	*0.5*	*0.4*	4.4	5.6	4.6	3.2	4.1
Sendai	2.4	2.9	2.8	1.4	2.4	1.2	1.6	1.7	0.9	0.9	3.1	3.6	3.8	2.0	3.2
Niigata*	2.0	2.2	2.6	1.4	1.8	1.9	2.6	2.7	0.8	1.6	2.2	2.3	2.7	1.8	1.8
Tokyo*	3.2	4.2	3.3	2.1	3.3	1.8	2.0	2.1	1.4	1.7	4.4	5.8	4.6	2.9	4.3
Yokohama	2.8	3.4	3.1	1.8	2.8	2.5	2.7	2.9	1.8	2.4	3.4	4.5	3.7	2.2	3.4
Nagoya	2.8	2.9	3.1	2.2	3.0	1.3	1.5	1.7	1.0	1.2	3.8	3.7	4.4	3.2	4.2
Kyoto	2.7	2.5	3.0	2.3	2.7	1.1	0.8	1.7	1.1	0.8	3.7	3.6	4.1	3.2	3.9
Osaka*	2.6	2.5	2.7	2.1	2.9	2.1	2.1	2.4	2.0	2.0	3.5	3.1	3.5	3.2	4.0
Hiroshima*	1.9	1.5	2.3	1.6	2.4	0.9	*0.6*	1.6	1.2	*0.4*	3.1	2.7	3.3	2.6	3.8
Fukuoka	3.0	2.8	3.4	2.2	3.7	1.7	1.6	2.1	1.4	1.6	4.9	4.2	5.8	3.7	6.0
Kagoshima*	2.5	2.4	2.8	2.0	2.8	1.2	1.1	1.6	1.1	1.3	3.9	3.5	4.4	3.3	4.6
15 stations*	1.5	1.5	1.9	1.1	1.4	1.1	1.1	1.6	0.8	0.8	1.8	1.8	2.1	1.6	1.8

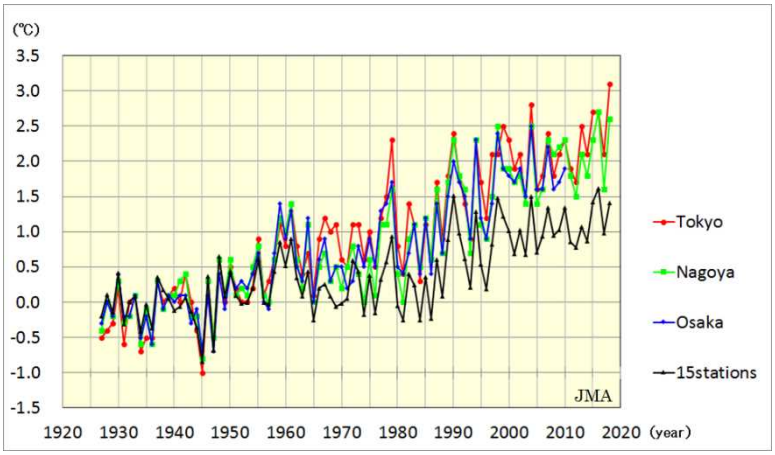

Figure 2.1-7 Annual temperature anomalies at Tokyo, Nagoya and Osaka and values averaged over 15 rural stations in Japan from 1927 to 2018

Anomalies are deviations from the baseline (i.e., the 1927 – 1956 average). Values averaged between 1927 and 1956 for respective stations all equal zero.

As it can be assumed that the long-term trends averaged over the 15 rural stations reflect large-scale climate change, the differences in the long-term trends of urban stations from the average of the 15 stations largely represent the influence of urbanization.

Detailed observation reveals that the long-term trends are more significant in winter, spring and autumn than in summer and more pronounced for minimum temperatures than for maximum temperatures at every urban observation station.

Records from urban stations whose data are not affected by relocation are used to determine long-term trends for the annual number of days with minimum temperatures of < 0°C and ≥ 25°C and maximum temperatures of ≥ 30°C and ≥ 35°C. The number of days with $T_{min} < 0$°C is very likely to have decreased with statistical significance at all urban stations, and the number with $T_{min} \geq 25$°C, $T_{max} \geq 30$°C and $T_{max} \geq 35$°C is very likely to have increased with statistical significance at most stations except Sapporo (Table 2.1-3).

Table 2.1-3 Long-term trends for the annual number of days with minimum temperatures of < 0°C and ≥ 25°C and maximum temperatures of ≥ 30°C and ≥ 35°C.

These figures are based on data from 1927 to 2018. The trend of the 13 rural station averages (Table 2.1-1, excluding Iida and Miyazaki) is also listed. Values shown in italics are not statistically significant at a confidence level of 90%.

Station	Annual number of days			
	Trend (days/decade)			
	$T_{min} < 0$°C	$T_{min} \geq 25$°C	$T_{max} \geq 30$°C	$T_{max} \geq 35$°C
Sapporo	−4.4	*0.0*	*0.1*	*0.0*
Sendai	−5.6	0.3	0.9	0.1
Yokohama	−6.0	3.0	2.2	0.2
Nagoya	−6.7	3.7	1.2	1.0
Kyoto	−7.1	3.6	1.3	1.3
Fukuoka	−4.9	4.7	1.1	1.1
13 Stations	−2.0	1.7	0.6	0.2

2.2 Changes in precipitation[16]

- The annual anomaly of global precipitation (for land areas only) in 2018 was +39 mm.
- The annual anomaly of precipitation in 2018 was +204.1 mm in Japan. Annual precipitation over Japan shows no discernible long-term trend.
- The annual number of days with daily and hourly extreme precipitation has increased in Japan, while that with wet days has decreased.
- Snow depth on the Sea of Japan side has decreased.

2.2.1 Global precipitation over land

Annual precipitation (for land areas only) in 2018 was +39 mm above the 1981 – 2010 average (Figure 2.2-1), and the figure has fluctuated periodically since 1901. In the Northern Hemisphere, records show large amounts of rainfall around 1930, in the 1950s and after the mid-2000s. Long-term trends are not analyzed because the necessary precipitation data for sea areas are not available.

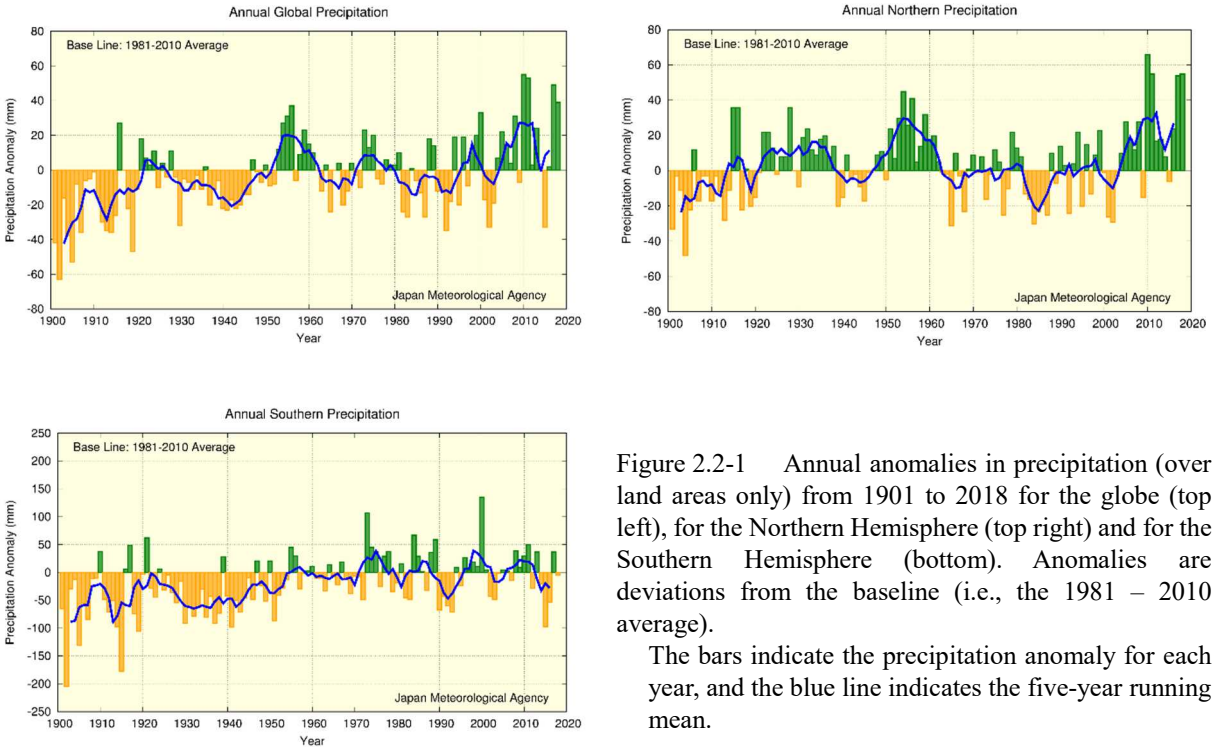

Figure 2.2-1 Annual anomalies in precipitation (over land areas only) from 1901 to 2018 for the globe (top left), for the Northern Hemisphere (top right) and for the Southern Hemisphere (bottom). Anomalies are deviations from the baseline (i.e., the 1981 – 2010 average).

The bars indicate the precipitation anomaly for each year, and the blue line indicates the five-year running mean.

2.2.2 Precipitation over Japan

This section describes long-term trends in precipitation over Japan as derived from analysis of precipitation records from 51 observation stations (Table 2.2-1).

Annual precipitation in 2018 was +204.1 mm above the 1981 – 2010 average. Japan experienced relatively large amounts of rainfall until the mid-1920s and around the 1950s. The annual figure exhibits greater variability for the period from the 1970s to the 2000s (Figure 2.2-2).

16 Data on annual precipitation around the world and in Japan are published on JMA's website. https://www.data.jma.go.jp/cpdinfo/temp/index.html (Japanese)

Table 2.2-1 List of 51 observation stations whose data are used to calculate precipitation anomalies and long-term trends in Japan

Element	Observation stations
Precipitation (51 stations)	Asahikawa, Abashiri, Sapporo, Obihiro, Nemuro, Suttsu, Akita, Miyako, Yamagata, Ishinomaki, Fukushima, Fushiki, Nagano, Utsunomiya, Fukui, Takayama, Matsumoto, Maebashi, Kumagaya, Mito, Tsuruga, Gifu, Nagoya, Iida, Kofu, Tsu, Hamamatsu, Tokyo, Yokohama, Sakai, Hamada, Kyoto, Hikone, Shimonoseki, Kure, Kobe, Osaka, Wakayama, Fukuoka, Oita, Nagasaki, Kumamoto, Kagoshima, Miyazaki, Matsuyama, Tadotsu, Kochi, Tokushima, Naze, Ishigakijima, Naha

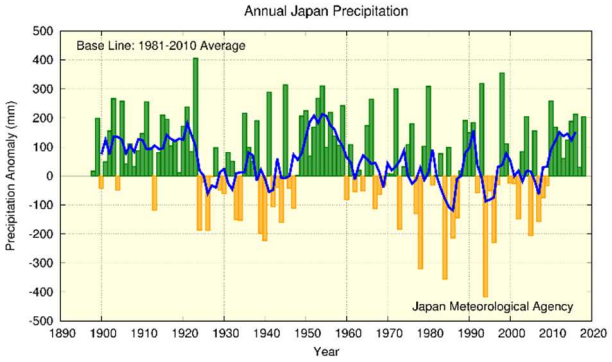

Figure 2.2-2 Annual anomalies in precipitation from 1898 to 2018 in Japan. Anomalies are deviations from the baseline (i.e., the 1981 – 2010 average).
The bars indicate the precipitation anomaly for each year, and the blue line indicates the five-year running mean.

2.2.3 Long-term trends of extreme precipitation events in Japan

This section describes long-term trends in frequencies of extremely wet/dry months and heavy daily precipitation events in Japan based on analysis of precipitation data from 51 observation stations.

(1) Extremely wet/dry months[17]

It is virtually certain that the frequency of extremely dry months increased during the period from 1901 to 2018 (statistically significant at a confidence level of 99%) (Figure 2.2-3 left). There has been no discernible trend in the frequency of extremely wet months (Figure 2.2-3 right).

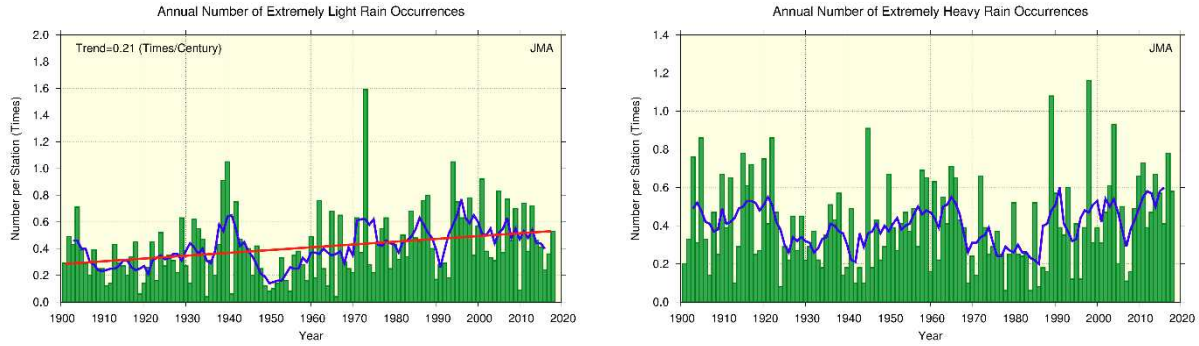

Figure 2.2-3 Annual number of extremely wet/dry months from 1901 to 2018
The graphs show the annual number of occurrences of the first-to-forth heaviest/lightest precipitation values for each month during the period from 1901 to 2018. The green bars indicate annual occurrences of extremely heavy/light monthly precipitation divided by the total number of monthly observation data sets available for the year (i.e., the average occurrence per station). The blue line indicates the five-year running mean, and the straight red line indicates the long-term liner trend.

17 Here, judgment of extremely heavy/light precipitation is based on the fourth–highest/lowest monthly values on record over the 118-year period from 1901 to 2018. The frequency of occurrence of the highest/lowest to the fourth–highest/lowest values over this period is once approximately every 30 years, which is close to JMA's definition of extreme climate events as those occurring once every 30 years or longer (See the Glossary for terms relating to Extreme climate event).

(2) Annual number of days with precipitation of ≥ 100 mm, ≥ 200 mm and ≥ 1.0 mm

The annual number of days with precipitation of ≥ 100 mm and ≥ 200 mm are virtually certain to have increased (both statistically significant at a confidence level of 99%) during the period from 1901 to 2018 (Figure 2.2-4) . The annual number of days with precipitation of ≥ 1.0 mm (Figure 2.2-5) is virtually certain to have decreased over the same period (statistically significant at a confidence level of 99%). These results suggest decrease in the annual number of wet days including light precipitation and in contrast, an increase in extremely wet days.

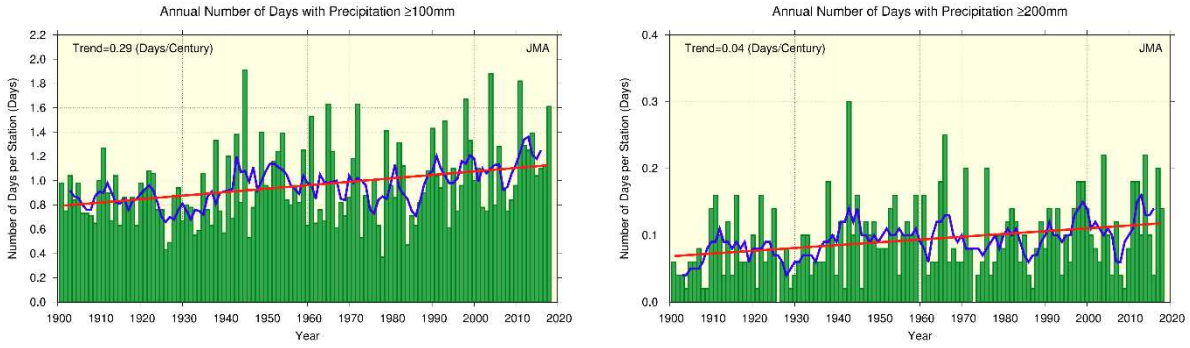

Figure 2.2-4 Annual number of days with precipitation ≥ 100 mm and ≥ 200 mm from 1901 to 2018
The green bars indicate the annual number of days per station for each year. The blue line indicates the five-year running mean, and the straight red line indicates the long-term liner trend.

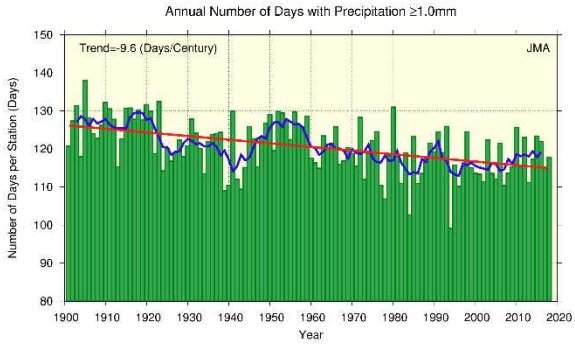

Figure 2.2-5 Annual number of days with precipitation of ≥ 1.0 mm from 1901 to 2018
As per figure 2.2-4.

2.2.4 Long-term trends of heavy rainfall analyzed using AMeDAS data

JMA operationally observes precipitation at about 1,300 unmanned regional meteorological observation stations all over Japan (collectively known as the Automated Meteorological Data Acquisition System, or AMeDAS). Observation was started in the latter part of the 1970s at many points, and observation data covering the approximately 40-year period through to 2018 are available[18]. Although the period covered by AMeDAS observation records is shorter than that of Local Meteorological Observatories or Weather Stations (which have observation records for the past 100 years or so), there are around eight times as many AMeDAS stations as Local Meteorological Observatories and Weather Stations combined. Hence, AMeDAS is better equipped to capture heavy precipitation events that take place on a limited spatial scale.

It is virtually certain that the annual numbers of events with precipitation of ≥ 50 mm and

18 The number of AMeDAS station was about 800 in 1976, and had gradually increased to about 1,300 in 2018. To account for these numerical differences, the annual number of precipitation events needs to be converted to a per-1,300-station basis. Data from wireless robot precipitation observation stations previously deployed in mountainous areas are also excluded.

≥ 80 mm per hour have increased (both statistically significant at a confidence level of 99%) (Figure 2.2-6). For the annual number of days with precipitation of ≥ 50 mm per hour, the number averaged for the last 10 years of the records (2009 – 2018) is about 311 on a per-1,300-station basis, which is about 1.4 times as many as that averaged for the first 10 years (1976 – 1985) of about 226.

The annual number of days with precipitation of ≥ 200 mm is very likely to have increased (statistically significant at a confidence level of 90%), and the corresponding figure for days with precipitation of ≥ 400 mm is extremely likely to have increased (statistically significant at a confidence level of 95%) (Figure 2.2-7).

As the annual number of extreme precipitation events is subject to large annual variations and the period covered by observation records is still relatively short, the addition of future observations to the data series is expected to increase the reliability of statistical trend detection.

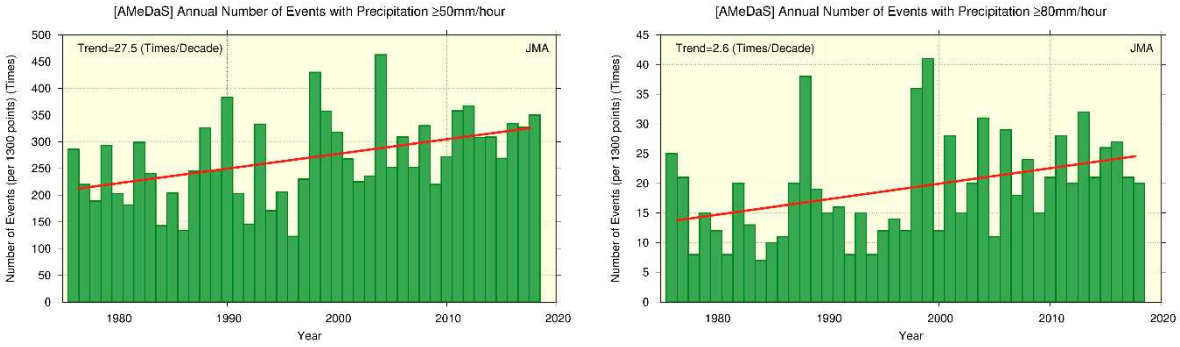

Figure 2.2-6 Annual number of events with precipitation of ≥ 50 mm and ≥ 80 mm per hour from 1976 to 2018
The green bars indicate the annual number of events per 1,300 AMeDAS stations for each year, and the straight red line indicates the long-term liner trend.

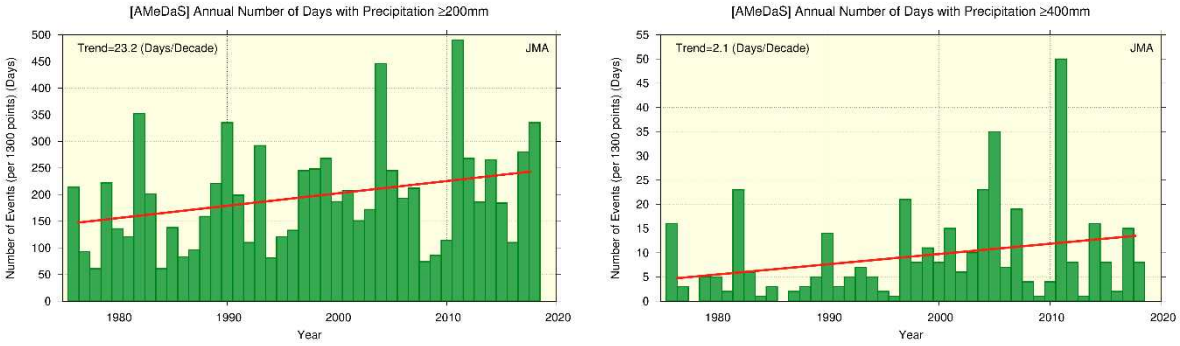

Figure 2.2-7 Annual number of days with precipitation of ≥ 200 mm and ≥ 400 mm from 1976 to 2018
The green bars indicate the annual number of days per 1,300 AMeDAS stations for each year, and the straight red line indicates the long-term liner trend.

2.2.5 Snow depth in Japan

Long-term trends in the annual maximum snow depth (represented in terms of a ratio against the 1981 – 2010 average) in Japan since 1962 are analyzed using observational records from stations located on the Sea of Japan coast (Table 2.2-2).

Table 2.2-2 Observation stations whose data are used to calculate snow depth ratios in Japan

Region	Observation stations
Sea of Japan side of northern Japan	Wakkanai, Rumoi, Asahikawa, Sapporo, Iwamizawa, Suttsu, Esashi, Kutchan, Wakamatsu, Aomori, Akita, Yamagata
Sea of Japan side of eastern Japan	Wajima, Aikawa, Niigata, Toyama, Takada, Fukui, Tsuruga
Sea of Japan side of western Japan	Saigo, Matsue, Yonago, Tottori, Toyooka, Hikone, Shimonoseki, Fukuoka, Oita, Nagasaki, Kumamoto

The annual maximum snow depth ratio in 2018 was 115% relative to the 1981 – 2010 average for the Sea of Japan side of northern Japan, 164% for the same side of eastern Japan, and 154% for the same side of western Japan (Figure 2.2-8). On a longer time scale, the annual maximum snow depth ratio from 1962 onward on the Sea of Japan side of northern Japan is very likely to have decreased at rates of 2.9% per decade (statistically significant at a confidence level of 90%), that on the Sea of Japan side of eastern Japan is extremely likely to have decreased at rates of 10.6% per decade (statistically significant at a confidence level of 95%), and that on the Sea of Japan side of western Japan is extremely likely to have decreased at rates of about 12.3% per decade (statistically significant at a confidence level of 95%). The annual maximum snow depth reached a local peak in the early 1980s followed by a sharp decline until around the early 1990s. The decline was particularly striking on the Sea of Japan side of eastern and western Japan.

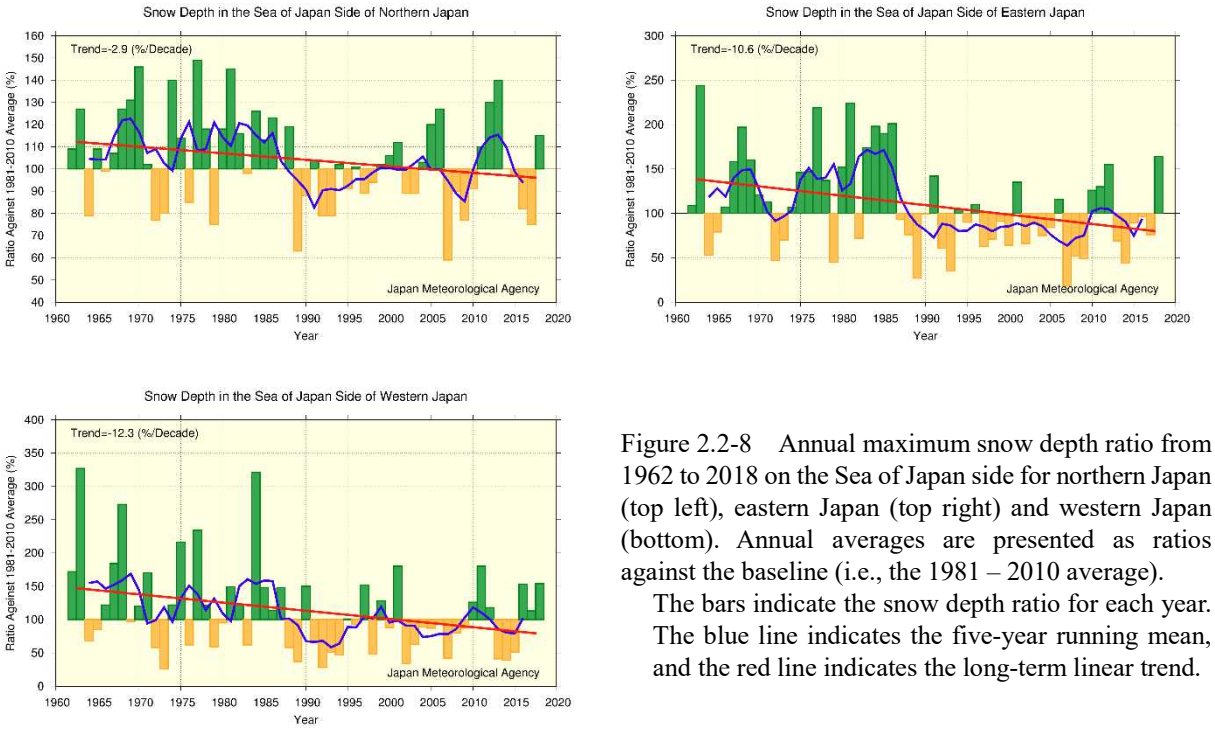

Figure 2.2-8 Annual maximum snow depth ratio from 1962 to 2018 on the Sea of Japan side for northern Japan (top left), eastern Japan (top right) and western Japan (bottom). Annual averages are presented as ratios against the baseline (i.e., the 1981 – 2010 average).
The bars indicate the snow depth ratio for each year. The blue line indicates the five-year running mean, and the red line indicates the long-term linear trend.

2.3 Changes in the phenology of cherry blossoms and acer leaves in Japan

- ○ It is virtually certain that cherry blossoms have been flowering earlier.
- ○ It is virtually certain that acer leaves have been changing color later.

JMA implements phenological observation to research the impact of meteorological condition on plants and animals, and eventually to monitor the progress of seasons as well as geographical variations and long-term changes in relation to the climate. Observation covers the first/full flowering and leaf color change of several plants and the first reported appearance/song of insects, birds and animals.

As part of its phenological monitoring, JMA observes cherry blossoms at 58 stations and acer leaves at 51 stations. Figure 2.3-1 shows interannual changes in the first reported dates of cherry blossom flowering and acer leaf color change between 1953 and 2018. The former exhibits a long-term advancing trend at a rate of 1.0 days per decade, while the latter shows a delaying trend at a rate of 2.8 days per decade (99% level of confidence for both cases). Table 2.3-1 compares climatological normals (based on 30-year averages) of the first reported date of cherry blossom flowering between 1961 – 1990 and 1981 – 2010 at stations in major Japanese cities. These phenomena are closely related to the surface mean temperature in the period before the event, and long-term warming is considered to be a major factor behind the trends observed.

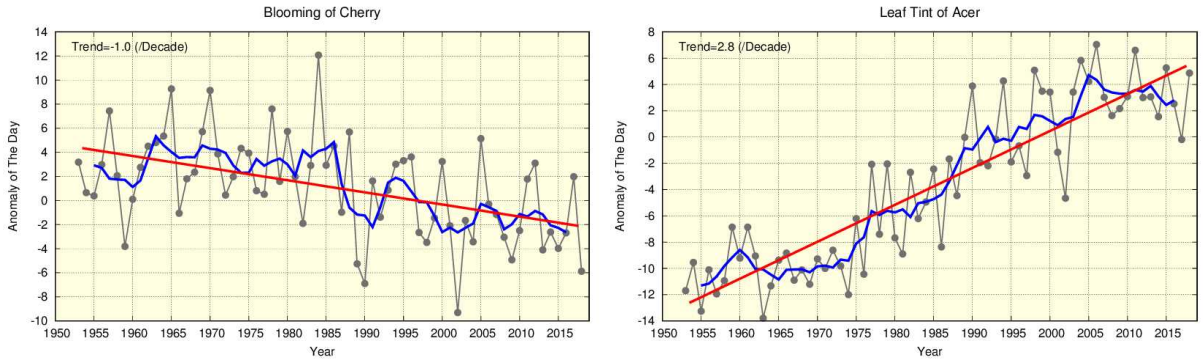

Figure 2.3-1 First reported dates of cherry blossom flowering (left) and acer leaf color change (right)
The black lines show annual anomalies of the first reported date averaged over all observation stations nationwide based on the normals for 1981 – 2010, and the blue lines indicate five-year running means. The red lines show the linear trend (cherry blossoms: −1.0 days per decade; acer leaves: +2.8 days per decade).

Table 2.3-1 Comparison of first reported dates of cherry blossom flowering
Differences in climatological normals for the first reported date of cherry blossom flowering between 1981 – 2010 and 1961 – 1990 at stations in major Japanese cities

Station	1961-1990 average	1981-2010 average	Difference (days)		1961-1990 average	1981-2010 average	Difference (days)
Kushiro	May 19	May 17	-2	Osaka	Apr 1	Mar 28	-4
Sapporo	May 5	May 3	-2	Hiroshima	Mar 31	Mar 27	-4
Aomori	Apr 27	Apr 24	-3	Takamatsu	Mar 31	Mar 28	-3
Sendai	Apr 14	Apr 11	-3	Fukuoka	Mar 28	Mar 23	-5
Niigata	Apr 13	Apr 9	-4	Kagoshima	Mar 27	Mar 26	-1
Tokyo	Mar 29	Mar 26	-3	Naha	Jan 16	Jan 18	+2
Nagoya	Mar 30	Mar 26	-4	Ishigakijima	Jan 15	Jan 16	+1

2.4 Tropical cyclones over the western North Pacific and the South China Sea

- A total of 29 tropical cyclones (TCs) with maximum wind speeds of 34 kt[19] or higher formed over the western North Pacific and the South China Sea in 2018, which was above normal.
- The numbers of formations show no significant long-term trend.

In 2018, 29 tropical cyclones (TCs) with maximum wind speeds of ≥ 34 kt formed over the western North Pacific and the South China Sea (Figure 2.4-1), which was above the normal (i.e., the 1981 – 2010 average) of 25.6. The numbers of formations show no discernible long-term trend during the analysis period from 1951 to 2018, but have often been lower since the latter half of the 1990s than in previous years. Numbers of TCs with maximum wind speeds of ≥ 34 kt approaching and making landfall in Japan were 16 and 5 (Figure 2.4-2), both of which were above the normal of 11.4 and 2.7, respectively. The numbers of TCs approaching Japan also show no discernible long-term trend during the same period from 1951 to 2018.

Figure 2.4-3 shows the numbers and rates of strong TCs with maximum wind speeds of ≥ 64 kt to those with maximum wind speeds of ≥ 34 kt from 1977 (the year in which the collection of complete data on maximum wind speeds near TC centers began). The numbers of strong TCs show no discernible trend.

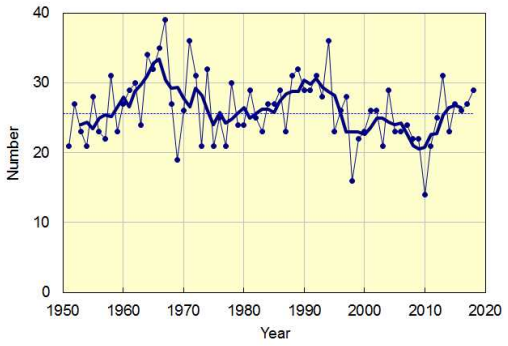

Figure 2.4-1 Time-series of the numbers of TCs with maximum wind speeds of ≥ 34 kt forming in the western North Pacific and the South China Sea from 1951 to 2018.
The thin and thick lines represent annual and five-year running means, respectively.

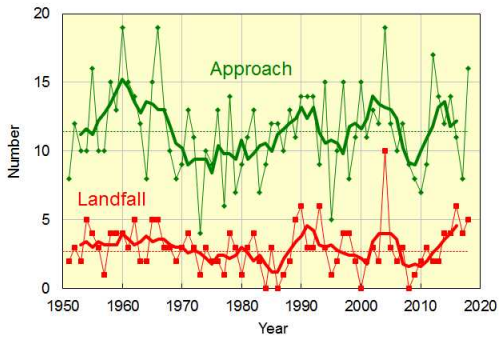

Figure 2.4-2 Time-series of the numbers of TCs with maximum wind speeds of ≥ 34 kt approaching (green) and making landfall in Japan (red) from 1951 to 2018.
The thin and thick lines represent annual and five-year running means, respectively.

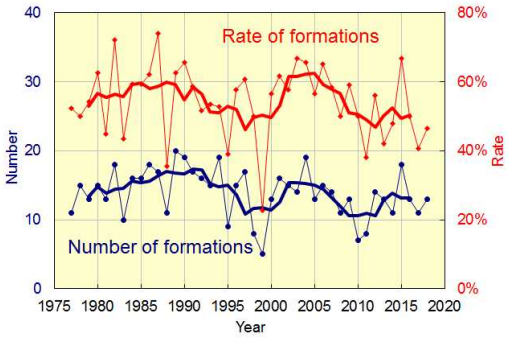

Figure 2.4-3 Time-series of the numbers of strong TCs with maximum wind speeds of ≥ 64 kt (blue) and rates of the strong TCs to the total TCs with maximum wind speeds of ≥ 34 kt (red) forming in the western North Pacific and the South China Sea from 1977 to 2018.
The thin and thick lines represent annual and five-year running means, respectively.

19 One knot (kt) is about 0.51 m/s

2.5 Sea surface temperature[20]

- The annual mean global average sea surface temperature (SST) in 2018 was 0.22°C above the 1981 – 2010 average, which was the fourth highest since 1891 (highest: 2016; second highest: 2015; third highest: 2017).
- The global average SST has risen at a rate of about +0.54°C per century.
- Annual average SSTs around Japan have risen by +1.12°C per century.

2.5.1 Global sea surface temperature

The annual mean global average SST in 2018 was 0.22°C above the 1981 – 2010 average. This was the fourth highest since 1891 (highest: 2016; second highest: 2015; third highest: 2017). The years from 2014 to 2018 represent the top-five five warmest since 1891.

The linear trend from 1891 to 2018 shows an increase of +0.54°C per century (Figure 2.5-1). Although magnitudes of the long-term SST trend vary by area, it is extremely likely that SSTs have increased in many parts of the world's oceans (Figure 2.5-2). Global average SSTs and global average surface temperatures (Section 2.1) are affected by natural climate variability on inter-annual to inter-decadal time scales as well as by global warming.

On a multi-year time scale, global average SSTs showed a rising trend from the middle of the 1970s to around 2000, before remaining largely static until the early 2010s and thereafter re-assuming an upward trend (Figure 2.5-1, blue line). This is partly because rising trends overlap with decadal-to-multi-decadal variations in the climate system. It is important to estimate the contribution of these internally induced natural variations in order to properly understand global warming. In the next section, the Pacific Decadal Oscillation (PDO) is presented as a typical example of decadal variability observed in SSTs.

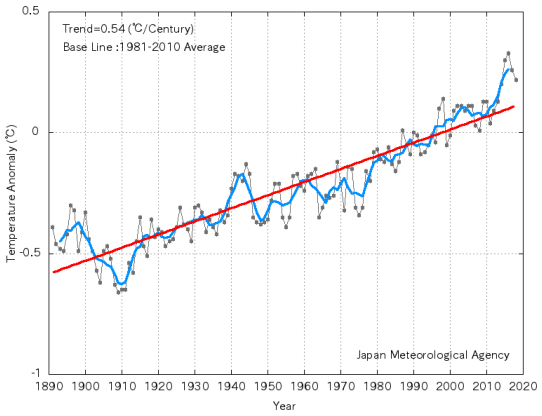

Figure 2.5-1 Time-series representation of global average sea surface temperature anomalies from 1891 to 2018

The black, blue and red lines indicate annual anomalies, the five-year running mean and the long-term linear trend, respectively. Anomalies are deviations from the 1981 – 2010 average.

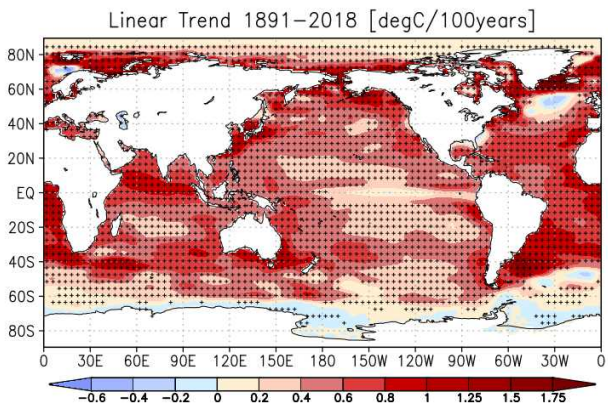

Figure 2.5-2 Linear trend of annual mean sea surface temperature during the period from 1891 to 2018 (°C per century)

Plus signs indicate statistically significant trends with a confidence level of 95%.

20 The results of analysis regarding tendencies of SSTs worldwide and around Japan are published on JMA's website.
https://www.data.jma.go.jp/gmd/kaiyou/english/long_term_sst_global/glb_warm_e.html
https://www.data.jma.go.jp/gmd/kaiyou/english/long_term_sst_japan/sea_surface_temperature_around_japan.html

2.5.2 Sea surface temperature (around Japan)

Figure 2.5-3 shows increase rates of area-averaged annual mean SSTs for 13 areas around Japan. The average SST of all areas around Japan has risen by +1.12°C per century, which is higher than the corresponding value for the North Pacific (+0.52°C per century).

It is virtually certain (statistically significant at a confidence level of 99%) that SSTs have risen by between +0.74 and +1.70°C per century in the sea off Kushiro, the sea off Sanriku, the southern part of the sea off Kanto, the sea off Shikoku and Tokai, the sea east of Okinawa, central and southwestern parts of the Sea of Japan, the Yellow Sea, the East China Sea, and the sea around the Sakishima Islands (areas E1-2, S1-3, N2-3, and W1-4). It is extremely likely (statistically significant at a confidence level of 95%) that SSTs in the eastern part of the sea off Kanto (area E3) have risen by +0.74°C per century. SSTs in the northeastern part of the Sea of Japan (area N1) exhibit no statistical long-term trend.

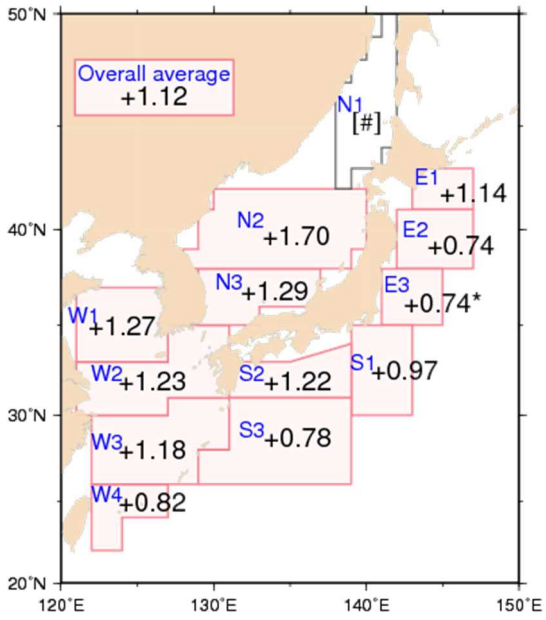

Area number	Area name
E1	Sea off Kushiro
E2	Sea off Sanriku
E3	Eastern part of the sea off Kanto
S1	Southern part of the sea off Kanto
S2	Sea off Shikoku and Tokai
S3	East of Okinawa
N1	Northeastern part of the Sea of Japan
N2	Central part of the Sea of Japan
N3	Southwestern part of the Sea of Japan
W1	Yellow Sea
W2	Northern part of the East China Sea
W3	Southern part of the East China Sea
W4	Sea around the Sakishima Islands

Figure 2.5-3 Increase rates of area-averaged annual mean SSTs around Japan from 1900 to 2018 (°C per century)
Areas with no symbol and those marked with [*] have statistical significant trend at confidence levels of 99% and 95%, respectively. Areas marked with [#] are those where no discernible trend is seen due to large SST variability factors such as decadal oscillation.

2.6 El Niño/La Niña [21] and PDO (Pacific Decadal Oscillation) [22]

- ○ The La Niña event that started in autumn 2017 ended in spring 2018. Thereafter, common characteristics of the past El Niño events have been observed in the equatorial Pacific since autumn 2018.
- ○ Negative PDO index values were generally observed from around 2000 to the early 2010s. Thereafter, the annual mean values have been consecutively positive since 2014, while the value approached zero in 2018.

2.6.1 El Niño/La Niña

An El Niño event is a phenomenon in which sea surface temperatures (SSTs) are above normal over the equatorial Pacific from near the date line to the coast of South America for around a year. In contrast, a La Niña event is a phenomenon in which SSTs are below normal over the same area. Both events occur every few years, causing changes in global atmospheric circulations which result in abnormal weather conditions worldwide. In Japan, cooler summers and warmer winters tend to appear during El Niño events, while hotter summers and colder winters tend to appear during La Niña events.

Figure 2.6-1 shows a time-series representation of SST deviations from climatological means based on a sliding 30-year period for the El Niño monitoring region (5°N – 5°S, 150°W – 90°W) and SST deviations from reference values based on linear extrapolation with respect to the latest sliding 30-year period for the tropical western Pacific region (Eq. – 15°N, 130 – 150°E) since 2008. SSTs in the El Niño monitoring region were below the relevant climatological means from January to April 2018 and have remained above these values since October 2018. SSTs in the Western Pacific region were above the related reference values from January to March of 2018, but have been below these levels since August 2018 except for October. These variations are consistent with the autumn 2017 termination of the La Niña event and the presence of El Niño-like characteristics events since autumn 2018.

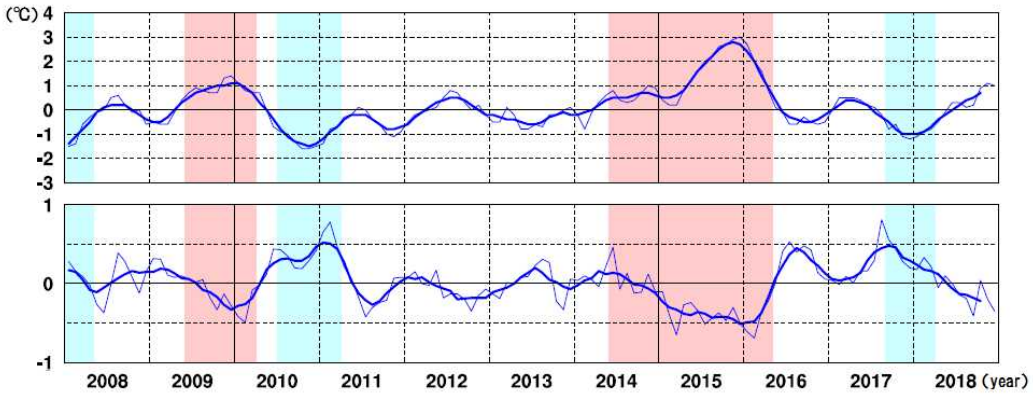

Figure 2.6-1 Time-series representations of SST deviations from the climatological mean based on a sliding 30-year period for the El Niño monitoring region (top) and SST deviations from reference values based on linear extrapolation with respect to the latest sliding 30-year period for the Western Pacific (bottom)
Thin lines indicate monthly means, and smooth thick curves indicate the five-month running mean.
Red shading denotes El Niño periods, and blue shading denotes La Niña periods.

21 See the Glossary for terms relating to El Niño phenomena. Monthly diagnosis reports, ENSO monitoring products, ENSO indices and El Niño outlooks are published on JMA's website.
https://ds.data.jma.go.jp/tcc/tcc/products/elnino/index.html
22 The PDO index time series is published on JMA's website.
https://ds.data.jma.go.jp/tcc/tcc/products/elnino/decadal/pdo.html

2.6.2 Pacific Decadal Oscillation

SST variability is also observed on time scales ranging from one to several decades in addition to El Niño/La Niña events, whose time scale is several years, and long-term trends associated with global warming. Among these, the atmosphere and oceans tend to co-vary with a period of more than ten years in the North Pacific in a phenomenon known as the Pacific Decadal Oscillation (PDO). When SSTs are lower (higher) than their normals in the central part of the North Pacific, those in its part along the coast of North America are likely to be higher (lower) than their normals. This seesaw pattern changes slowly, and appears repeatedly with a period of more than ten years. The PDO index, which is defined by the SST anomaly pattern in the North Pacific, is used as a measure of phase and strength of the oscillation. It is noted that both the PDO index and SST anomaly patterns associated with PDO include relatively short-timescale variabilities such as El Niño/La Niña events in addition to decadal to multi-decadal components.

When the PDO index is positive (negative), SSTs in the central part of the North Pacific are likely to be lower (higher) than their normals in addition to those along the coast of North America, and those in the equatorial part from near the date line to the coast of South America are likely to be higher (lower) than normal. This tendency is analogous to the patterns observed in El Niño (La Niña) events (Figure 2.6-2). Additionally, sea level pressures (SLPs) in the high latitudes of the North Pacific are likely to be lower (higher) than their normals in the same time (Figure 2.6-3). This indicates that the Aleutian Low is stronger (weaker) than its normal in winter and spring. These atmospheric variations affect meteorological conditions mainly in North America. When the PDO index is positive, winter temperatures tend to be high in the northwestern part of North America and the northern part of South America, and low in the southeastern part of the USA and in parts of China (Mantua and Hare, 2002).

The PDO index was generally positive from the late 1920s to the early 1940s and from the late 1970s to around 2000, and was generally negative from the late 1940s to the mid-1970s and from around 2000 to the early 2010s. The annual mean PDO index value has remained positive since 2014, although it was close to zero (+0.2) in 2018 (Figure 2.6-4).

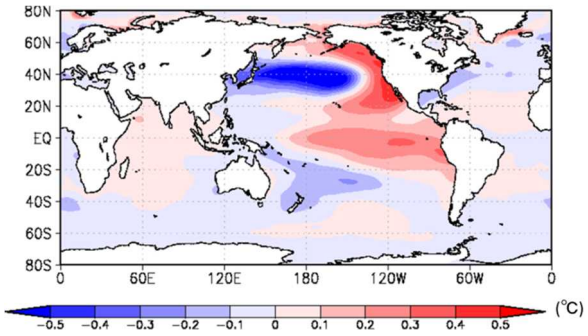

Figure 2.6-2 Typical SST anomaly patterns in the positive phase of the PDO

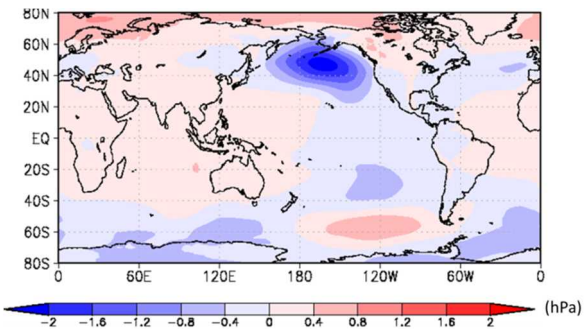

Figure 2.6-3 Typical SLP anomaly patterns in the positive phase of the PDO

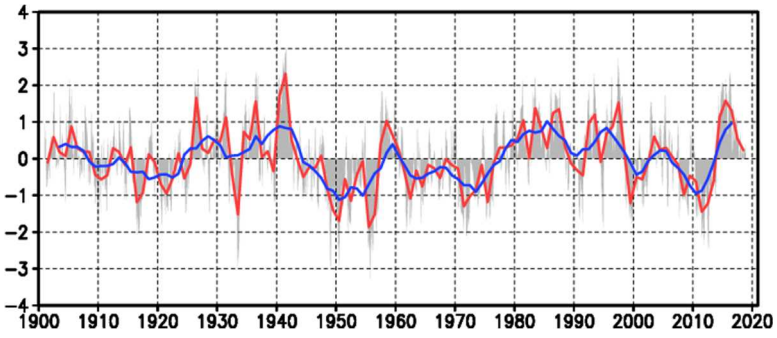

Figure 2.6-4 Time-series of the PDO index
The red line represents annual mean values for the PDO index, the blue line represents five-year running mean values, and the gray bars represent monthly values.

2.7 Global upper ocean heat content[23]

○ An increase in globally integrated upper ocean heat content was observed from 1950 to 2018 with a linear trend of 2.35×10^{22} J per decade.

Oceans have a significant impact on the global climate because they cover about 70% of the earth's surface and have high heat capacity. According to the Intergovernmental Panel on Climate Change Fifth Assessment report (IPCC, 2013), more than 60% of the net energy increase in the climate system from 1971 to 2010 is stored in the upper ocean (0 – 700 m), and about 30% is stored below 700 m. Oceanic warming results in sea level rises due to thermal expansion.

It is virtually certain that globally integrated upper-ocean (0 – 700 m) heat content (OHC) rose between 1950 and 2018 at a rate of 2.35×10^{22} J per decade as a long-term trend with interannual variations (statistically significant at a confidence level of 99%) (Figure 2.7-1). This trend corresponds to a rise of 0.025°C per decade in the globally averaged upper-ocean (0 – 700 m) temperature. OHC has exhibited marked increases since the mid-1990s. These long-term trends can be attributed to global warming caused by increased concentrations of anthropogenic greenhouse gases such as CO_2 as well as natural variability.

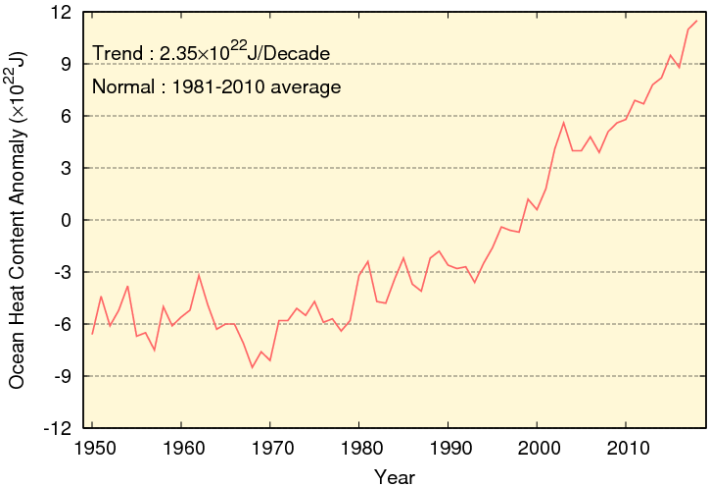

Figure 2.7-1 Time-series representation of the globally integrated upper ocean (0 – 700 m) heat content anomaly
The 1981 – 2010 average is referenced as the normal.

23 The results of ocean heat content analysis are published on JMA's website.
https://www.data.jma.go.jp/gmd/kaiyou/english/ohc/ohc_global_en.html

2.8 Sea levels around Japan [24]

- ○ A trend of sea level rise has been seen in Japanese coastal areas since the 1980s.
- ○ No trend of sea level rise was seen in Japanese coastal areas for the period from 1906 to 2018.

The IPCC Fifth Assessment Report 2013 (AR5) concluded that the global mean sea level had risen due mainly to 1) oceanic thermal expansion, 2) changes in mountain glaciers, the Greenland ice sheet and the Antarctic ice sheet, and 3) changes in land water storage. The report also said it is very likely that the mean rate of global average sea level rise was 1.7 [1.5 to 1.9] mm/year between 1901 and 2010, 2.0 [1.7 to 2.3] mm/year between 1971 and 2010, and 3.2 [2.8 to 3.6] mm/year between 1993 and 2010, where the values in square brackets show the 90% uncertainty range.

Sea levels in Japanese coastal areas exhibited no rise from 1906 to 2018 (Figure 2.8-1), but have shown a rising trend since the 1980s. Recent rates of rise around the country have been 1.1 [0.6 to 1.6] mm/year from 1971 to 2010 and 2.8 [1.3 to 4.3] mm/year from 1993 to 2010. These are comparable to the global average figures provided in AR5.

In Japanese coastal areas, variations with 10- to 20-year periods were between 1906 and 2018. The major factor behind sea level variations with 10- to 20-year periods is the variability of atmospheric circulation over the North Pacific. Westerlies in the mid-latitudes of the Northern Hemisphere are strengthened in boreal winter, and the consequent decadal variations in turn cause sea level variations in the central North Pacific. These propagate westward due to the earth's rotation, causing sea level rise around Japan.

The extent to which global warming has contributed to sea level change around Japan remains unclear due to the involvement of various other factors such as variations with 10- to 20-year periods as mentioned above. Continuous monitoring is needed to clarify the long-term trend of sea level rise caused by global warming.

24 Sea levels around Japan are published on the JMA's website.
https://www.data.jma.go.jp/gmd/kaiyou/english/sl_trend/sea_level_around_japan.html

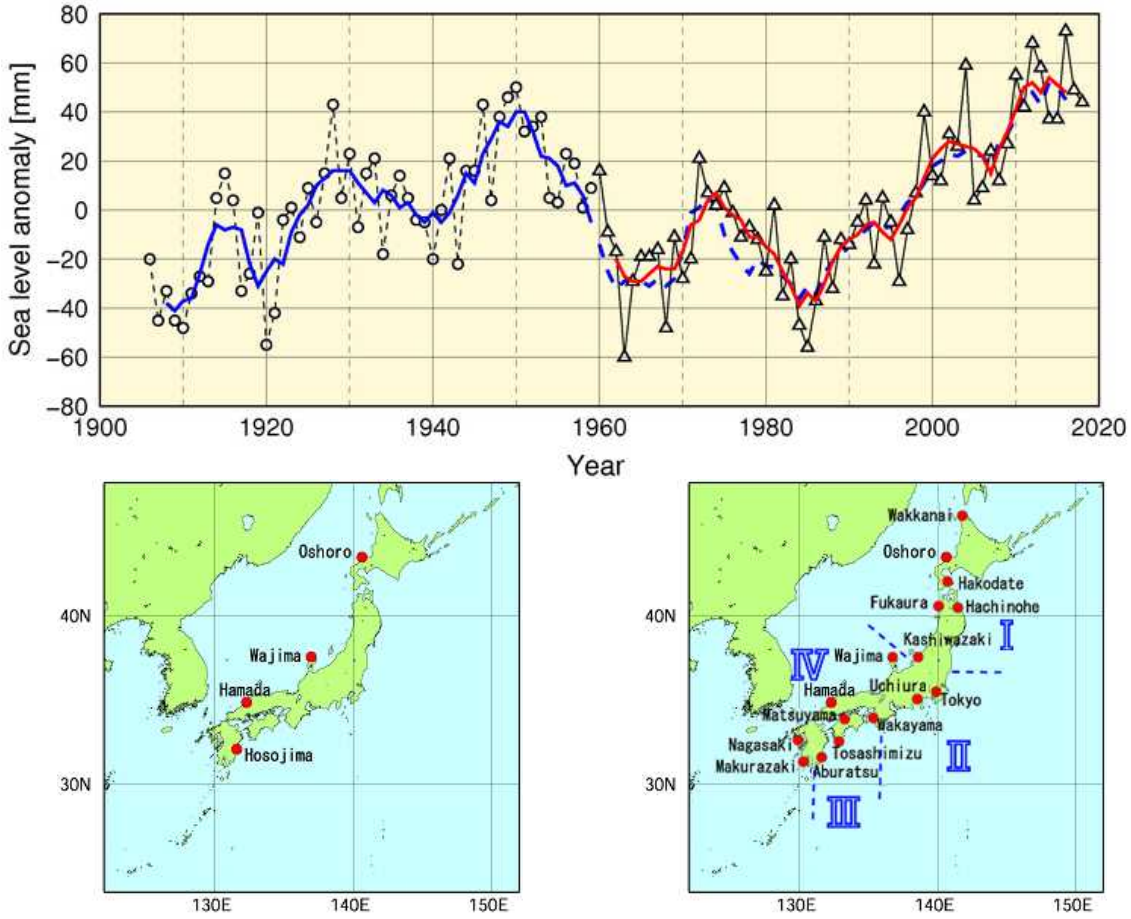

Figure 2.8-1 Time-series representation of annual mean sea levels (1906 – 2018) and locations of tide gauge stations

Tide gauge stations assessed as being affected to a lesser extent by crustal movement are selected. The four stations shown on the map on the left are used for the period from 1906 to 1959, and the sixteen shown on the right are used for the period since 1960. From 1906 to 1959, a time-series representation of mean annual mean sea level anomalies for the selected stations is shown. For the period since 1960, the nation's islands were then divided into four regions based on sea level variation characteristics, annual mean sea level anomalies were averaged for each of the regions, and the variations were plotted in the figure. The four regions are I: from Hokkaido to Tohoku district; II: from Kanto to Tokai district; III: from the Pacific coast of Kinki to that of Kyushu district; and IV: from Hokuriku to East China Sea coast of Kyushu district. Sea level variations are plotted on the chart as a time-series representation of annual mean sea level anomalies for each year, obtained using the 1981 to 2010 average as the normal. The solid blue line represents the five-year running mean of annual sea level anomalies averaged among the four stations shown in the lower left map, while the solid red line represents that averaged among the four divided regions in the lower right map. The dashed blue line represents the value averaged among the four stations shown in the lower left map for the same period shown by the solid red line (after 1960) for reference. The coefficient of correlation between the solid red line and the dashed blue line from 1962 to 2016 is as high as 0.98. Accordingly, the extent to which changing the tide gauge stations used in the monitoring affects the analysis of variance of sea level anomalies can be regarded as small. Among the tide gauge stations, those at Oshoro, Kashiwazaki, Wajima and Hosojima belong to the Geospatial Information Authority of Japan. Sea level data for the Tokyo station are available from 1968 onward. Sea level data for the period from 2011 to 2018 from Hakodate, Fukaura, Kashiwazaki, Tokyo and Hachinohe were not used due to possible influences from the 2011 off the Pacific coast of Tohoku Earthquake.

2.9 Sea ice[25]

○ The sea ice extent in the Arctic Ocean is decreasing. In 2018, the annual maximum sea ice extent in the Arctic Ocean was 14.60 × 10^6 km^2, which were the second-lowest value since 1979.
○ The sea ice extent in the Antarctic Ocean is extremely likely to be on an increasing trend, although values observed since 2016 have been lower than normal. In 2018, the annual minimum sea ice extent in the Antarctic Ocean was 2.32 × 10^6 km^2, which was the second lowest value since 1979.
○ The maximum sea ice extent in the Sea of Okhotsk shows a decreasing trend of 0.066 × 10^6 km^2 per decade.

2.9.1 Sea ice in Arctic and Antarctic areas (Figures 2.9-1, 2.9-2, 2.9-3)

Sea ice is formed when sea water in the Arctic and Antarctic freezes. As the albedo (reflection coefficient) of sea ice is greater than that of the ocean surface, sea ice extent reductions caused by global warming result in more solar energy absorption at the surface, which in turn accelerates global warming. Sea ice also affects deep-ocean circulation because the expelled salt as it forms increases the salinity (and therefore the density) of the water below it causing the water to sink.

It is virtually certain that there has been a long-term trend of decrease in sea ice extent in the Arctic Ocean since 1979, when continuous monitoring of sea ice using satellite sensors with similar properties started (statistically significant at a confidence level of 99%). In particular, the reduction in the annual minimum extent is notable. The rate of decrease in the annual minimum up to 2018 was 0.089 × 10^6 km^2 per year. Meanwhile, it is extremely likely that there has been a long-term trend of increase at a rate of 0.015 × 10^6 km^2 per year in the annual mean sea ice extent in the Antarctic Ocean (statistically significant at a confidence level of 95%). However, values observed since 2016 have been lower than normal (Figure 2.9-1).

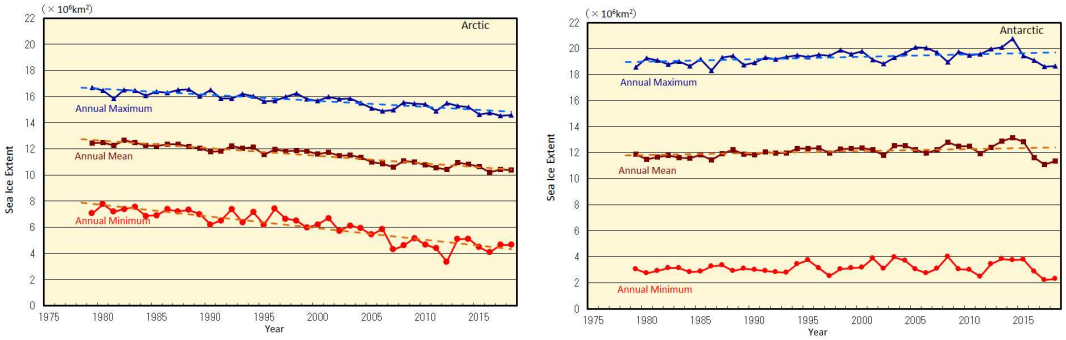

Figure 2.9-1 Time-series representations of annual maximum, annual mean and annual minimum sea ice extent in the Arctic Ocean (including the Sea of Okhotsk and the Bering Sea) (left) and in the Antarctic Ocean (right) from 1979 to 2018

The solid blue, brown and red lines indicate the annual maximum, the annual mean and the annual minimum sea ice extent, respectively. The dashed lines indicate the linear trends. Sea ice extents are calculated from brightness temperature data provided by NASA (the National Aeronautics and Space Administration) and NSIDC (the National Snow and Ice Data Center).

25 Information on sea ice in the Arctic/Antarctic, and in the Sea of Okhotsk are published on JMA's website.
https://www.data.jma.go.jp/gmd/kaiyou/english/seaice_global/series_global_e.html (Arctic/Antarctic)
https://www.data.jma.go.jp/gmd/kaiyou/english/seaice_okhotsk/series_okhotsk_e.html (Sea of Okhotsk)

In 2018, the annual maximum Arctic sea ice extent was 14.60 × 10^6 km^2 on March 16, marking the second-lowest value after 2017 since 1979. The extent subsequently decreased during spring and summer in the Northern Hemisphere and reached its annual minimum of 4.66 × 10^6 km^2 on September 17, marking the eighth-lowest value since 1979. Meanwhile, the Antarctic sea ice extent was at its annual minimum of 2.32 × 10^6 km^2 on February 18, also marking the second-lowest value after 2017 since 1979. The extent subsequently increased during the autumn and winter months of the Southern Hemisphere and reached its annual maximum of 18.65 × 10^6 km^2 on September 30, marking the fourth-lowest value since 1979 (Figures 2.9-1, 2.9-2, 2.9-3).

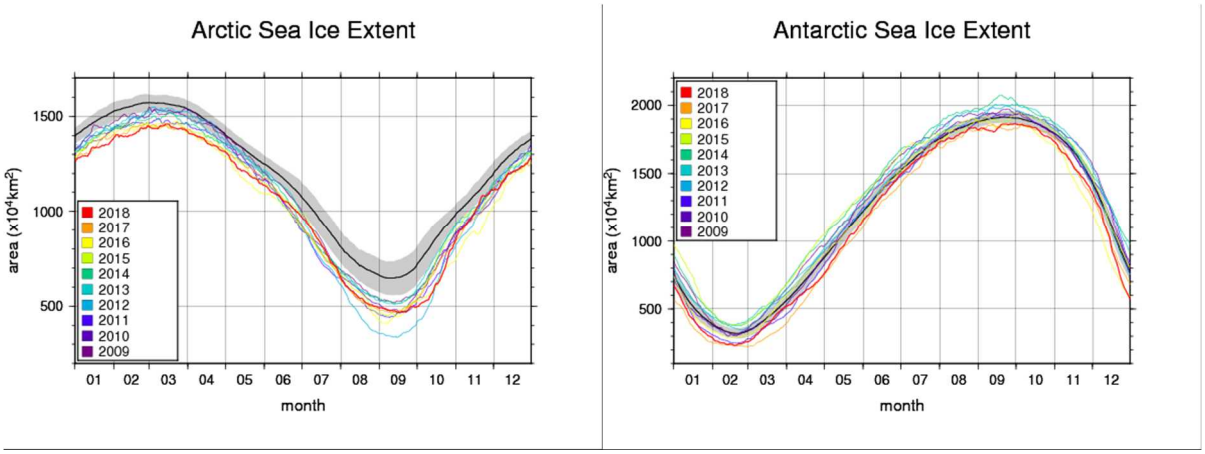

Figure 2.9-2 Annual variations of sea ice extent in the Arctic (left) and Antarctic (right) areas in 2018 (red line) Black lines represent the normal, and shading represents the range of the normal.

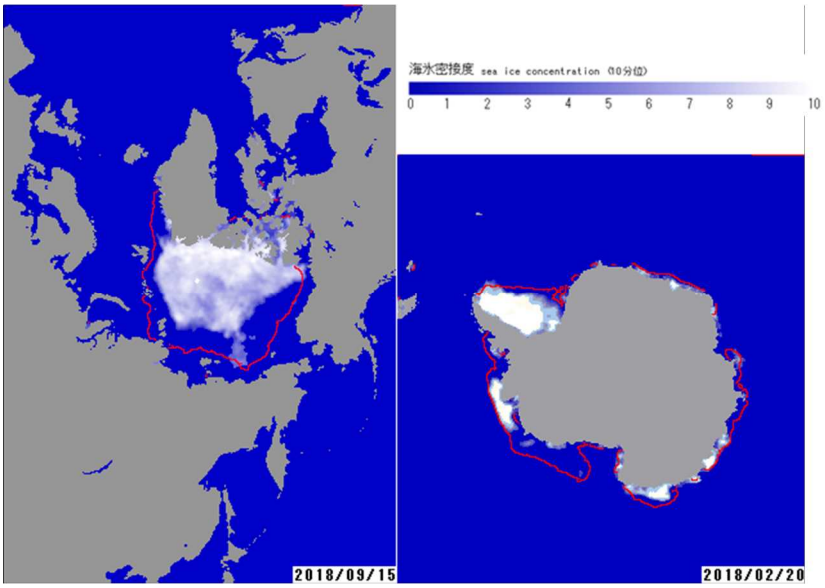

Figure 2.9-3 Annual minimum sea ice distribution for the Arctic and Antarctic

The figure on the left shows Arctic sea ice concentration on September 15 2018, and on the right is Antarctic sea ice concentration on February 20 2018. The red lines represent the normal sea ice edge for the relevant days.

2.9.2 Sea ice in the Sea of Okhotsk (Figure 2.9-4)

The Sea of Okhotsk is the southernmost sea in the Northern Hemisphere where sea ice is observed across a wide area. The variation of the sea ice in the Sea of Okhotsk has effect on climate in coastal area facing the Sea of Okhotsk in Hokkaido and water quality of Oyashio.

The maximum[26] sea ice extent in the Sea of Okhotsk shows large interannual variations. However, it is virtually certain that it exhibited a long-term trend of decrease for the period from 1971 to 2018 (statistically significant at the confidence level of 99%). The maximum extent has decreased by 0.066×10^6 km^2 per decade (corresponding to 4.2% of the Sea of Okhotsk's total area).

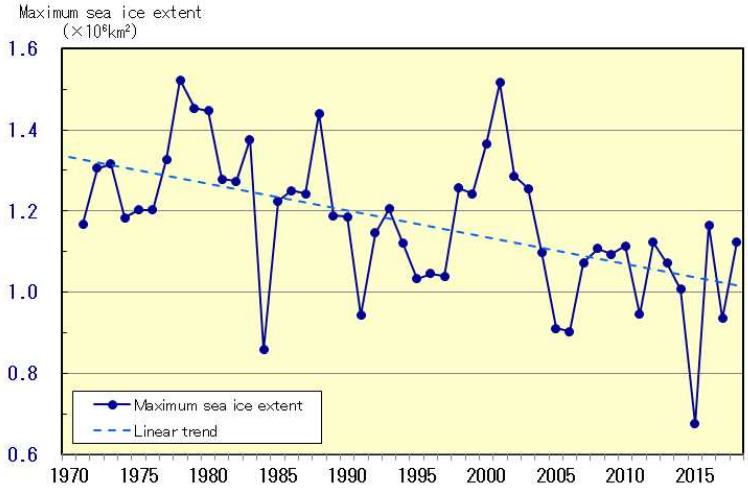

Figure 2.9-4 Time-series representations of maximum sea ice extent for the Sea of Okhotsk from 1971 to 2018
Straight line indicates the linear trend.

26 The maximum sea ice extent: It shows sea ice extent that sea ice was the most expanding of every five days in the winter.

2.10 Snow cover in the Northern Hemisphere

- It is extremely likely that a decreasing trend is observed in the interannual variability of the total snow cover extent in the Northern Hemisphere for January, June and the period from September to December and in Eurasia for April, June and the period from September to December.
- In winter 2017/2018, there were more days of snow cover than normal over the central part of North America and Europe, and fewer over the western part of North America and from Central Asia to East Asia.

JMA monitors snow-cover variations in the Northern Hemisphere using analysis data from satellite observations[27] based on its own algorithm. The average seasonal migration of snow cover in the Northern Hemisphere normally peaks around January – February and decreases in spring.

In the Northern Hemisphere (north of 30°N), it is extremely likely (statistically significant at a confidence level of 95%) that a decreasing trend is observed in the interannual variability of the total snow cover extent over the 31-year period from 1988 to 2018 for January, June and the period from September to December, while no discernible trend is seen for the period from February to May (Figure 2.10-1 (a) and (c)). In Eurasia (north of 30°N from 0° to 180°E), it is extremely likely (statistically significant at a confidence level of 95%) that a decreasing trend is observed in the interannual variability of the total snow cover for April, June and the period from September to December, while no discernible trend is seen for the period from January to March and May (Figure 2.10-1 (b) and (d)). In winter (December to February) 2017/2018, there were more days of snow cover than normal over the central part of North America and Europe, and fewer over the western part of North America and from Central Asia to East Asia (Figure 2.10-1 (e)). In November 2018, there were more days of snow cover than normal over North America and Central Asia, and fewer from eastern Europe to western Russia and over East Asia (Figure 2.10-1 (f)).

The albedo of snow-covered ground (i.e., the ratio of solar radiation reflected by the surface) is higher than that of snow-free ground. The variability of snow cover has an impact on the earth's surface energy budget and radiation balance, and therefore on the climate. In addition, snow absorbs heat from its surroundings and melts, thereby providing soil moisture and related effects on the climate system. The variability of atmospheric circulation and oceanographic conditions affects the amount of snow cover, which exhibits a close and mutual association with climatic conditions. Snow-cover variations in Eurasia and other parts of the Northern Hemisphere may affect climate conditions in Japan, but the mechanisms behind such a potential influence remain unclear. The accumulation of future observation data in addition to the current body of information and the implementation of related research are expected to increase the reliability of statistical work to identify trends of snow cover extent and help to elucidate how snow-cover variations affect climate conditions.

27 The Defense Meteorological Satellite Program (DMSP) polar-orbiting satellites of the USA, equipped with the Special Sensor Microwave/Imager (SSM/I) and the Special Sensor Microwave Imager Sounder (SSMIS)

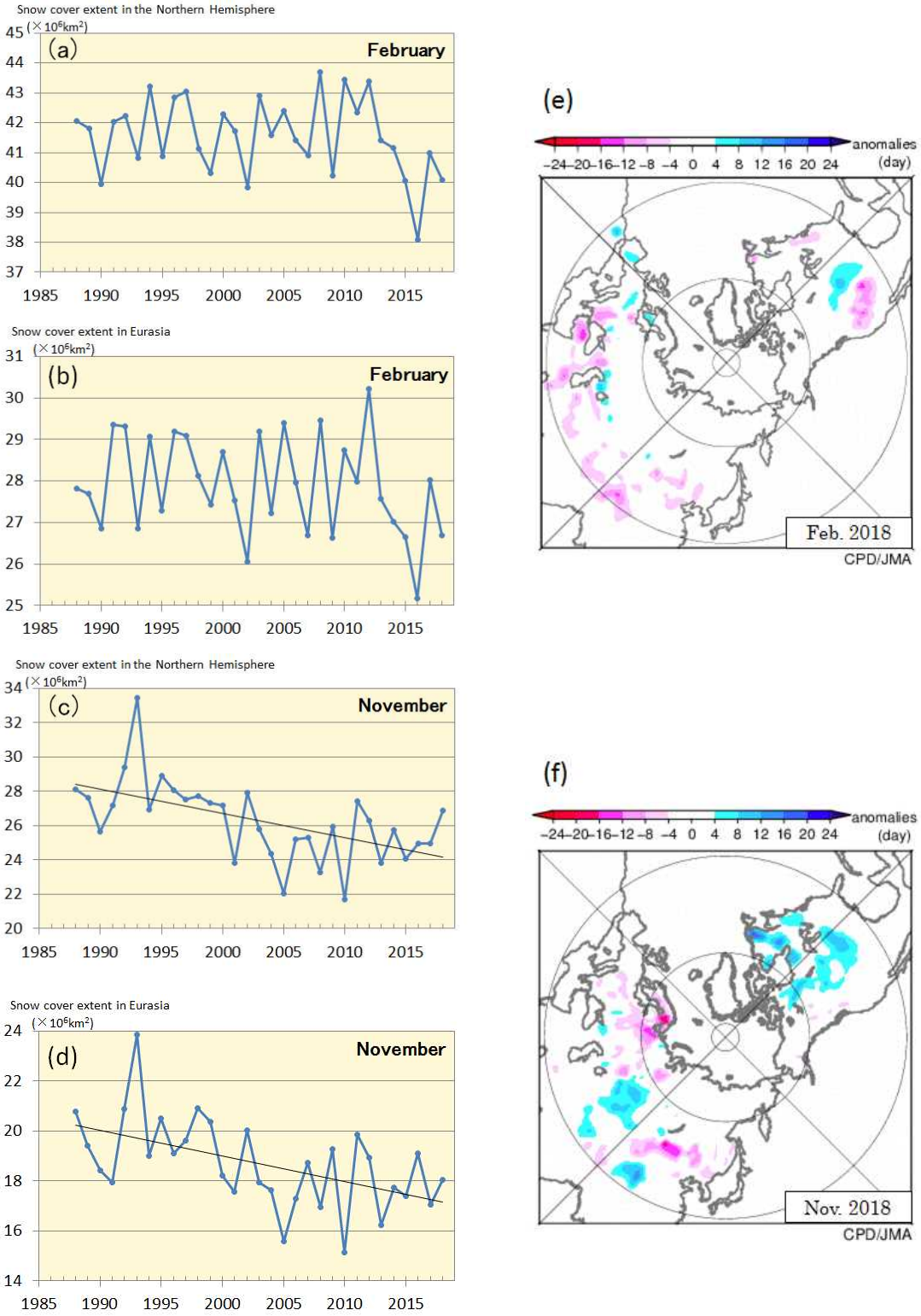

Figure 2.10-1 Interannual variations in the total area of monthly snow cover (km^2) in the Northern Hemisphere (north of 30°N) for (a) February and (c) November and in Eurasia (north of 30°N, from 0° to 180°E) for (b) February and (d) November from 1988 to 2018, and anomalies in the number of days with snow cover for (e) February and (f) November in 2018

(a) - (d): The blue lines indicate the total snow cover area for each year, and the black lines show linear trends (statistically significant at a confidence level of 95%).

(e) - (f): Blue (red) shading indicates more (fewer) days of snow cover.

The base period for the normal is 1989 – 2010.